Nucleation of Ga_2O_3 nanocrystals in the $K_2O-Ga_2O_3-SiO_2$ glass system

R. Ceccato, R. Dal Maschio, and S. Gialanella
Dipartimento di Ingegneria dei Materiali, Università di Trento, 38050 Mesiano, Trento, Italy

G. Mariotto,[a] M. Montagna, and F. Rossi
Instituto Nazionale per la Fisica della Materia and Dipartimento di Fisica, Università di Trento, Via Sommarive, 14-38050 Povo, Trento, Italy

M. Ferrari
Centro di Fisica degli Stati Aggregati, Consiglio Nazionale delle Ricerche, Via Sommarive, 14-38050 Povo, Trento, Italy

K. E. Lipinska-Kalita and Y. Ohki
Department of Electrical, Electronic, and Computing Engineering, Washeda University, 4-4-1 Ohkubo, Shinjuku, Tokyo 169-8555 Japan

(Received 16 October 2000; accepted for publication 20 February 2001)

A multitechnique approach, consisting of x-ray diffraction, differential thermal analysis, low frequency Raman scattering from the acoustic vibrations of nanoclusters, and transmission electron microscopy associated with selected area diffraction, has been used to study the nucleation and crystallization processes in $SiO_2-Ga_2O_3-K_2O$ glasses. The specific aim was to determine the structure and the size distribution of nanoparticles embedded in the glass matrix. It has been found that nearly spherical nanocrystals of β-Ga_2O_3, with a size of $\sim 2-3$ nm, nucleate during thermal treatments at 900 °C. Crystallization was observed after annealing at higher temperature. The amount of the crystalline phase and the mean size of the nanocrystals increased with heat treatment, time and temperature. β-Ga_2O_3 was the only crystalline phase to appear in all glass samples. [DOI: 10.1063/1.1365426]

I. INTRODUCTION

Studies of nucleation and crystallization processes in glasses are interesting both for their fundamental physics and technological applications. In particular, the devitrification process of glasses is an important problem related to the fabrication of optical fibers or to the synthesis of lasing materials.[1–5] On the other hand, it would certainly be advantageous for some applications to obtain optically active nanocrystals embedded in a silicate glass matrix. The crystalline environment of the optically active ion could avoid fluorescence quenching and provide large cross sections for absorption and stimulated emission.[1,4,5] Small sized crystallites are required to avoid Rayleigh scattering losses. The host silicate glass, in the form of a planar waveguide, is compatible with fiber coupling and can be used in integrated optics.[6,7]

Investigations of early stages of crystallization in oxide glasses were carried out by using different spectroscopic methods based on local probes, like Raman scattering, luminescence, or electron microscopy.[8–11] In particular, low frequency Raman scattering is very sensitive to structural features at the scale of few nanometers, i.e., an intermediate one between molecular and bulk regimes.[8,12,13]

Alkali galliosilicate glasses, structurally isomorphic to alkali aluminosilicate glasses, were studied in detail by Shelby *et al.*[14–18] and the local structure around the gallium atoms has been determined by means of an EXAFS study carried out on a set of samples with different compositions. Structural studies of an isomorphic series of glasses from the system $SiO_2/Ge_2O-Al_2O_3/Ga_2O_3-K_2O$ were performed by Lipinska-Kalita *et al.*[19,20] using vibrational and Mossbauer spectroscopy.

In this work we focus on the study of the very early stages of crystallization in the $SiO_2-Ga_2O_3-K_2O$ glass system, with the aim of obtaining optically transparent glass ceramics by controlled nucleation and crystallization.

II. EXPERIMENT

A. Sample preparation and thermal treatments

Glass of nominal composition

$$(K_2O)_{6.37}(Ga_2O_3)_{12.47}(SiO_2)_{81.13}$$

be (in mol %) was prepared by mixing pure, analytical grade K_2CO_3 and Ga_2O_3 powders with high purity SiO_2 powder (>99.6%). The mixture of reagents was melted within a platinum crucible in air at 1550 °C for 12 h, and then quenched by pouring onto a cold metal mold.

As-quenched samples were cut in small platelets of typical size $4\times6\times2$ mm^3 and then annealed at different temperatures up to 1150 °C in air with a heating rate changing from 0.4 °C/min (up to 200 °C) to 0.1 °C/min (from 700 °C to the setup temperature); a further isothermal treatment of 4 h was performed at the highest temperature of sample annealing.

[a]Author to whom correspondence should be addressed; electronic mail: mariotto@science.unitn.it

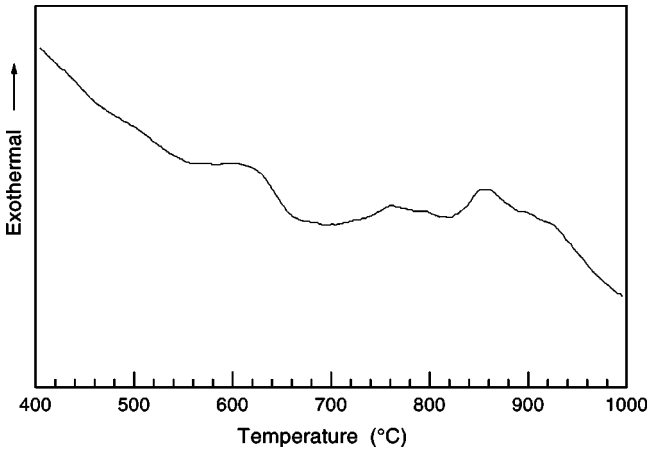

FIG. 1. DTA curve of the as-quenched glass.

B. Experimental methods

Differential thermal analysis (DTA) studies were performed using an STA-409 Netzsch instrument; powdered samples were heated up to 1350 °C with a heating rate of 10 °C/min in static air conditions.

X-ray diffraction (XRD) spectra were collected on a Rigaku diffractometer in θ-2θ Bragg–Brentano geometry using Cu $K\alpha$ radiation and a graphite monochromator in the diffracted beam.

Transmission electron micrographs (TEM) of the powdered samples spread over carbon coated copper grids were obtained by using a Philips 400 T microscope, operating at 120 kV.

VV and HV Raman scattering spectra of glass platelets, mounted into an evacuated optical cryostat at room temperature, were taken by using either the 488.0 or the 514.5 nm line of an Ar^+ ion laser with a power of 300 mW at the sample surface. The scattered light was collected at 90° to the incident beam and focused onto the entrance slit of a double monochromator (Jobin–Yvon, model Ramanor HG2-S) mounting concave holographic gratings (2000 lines/mm). The filtered radiation was detected by a cooled (−35 °C) photomultiplier tube operated in photon counting mode, which was interfaced to a multichannel analyzer and a personal computer.

Raman spectra were recorded with resolution of 0.5 to 3 cm^{-1}. The reproducibility of peak position and intensity was determined by taking independent measurements in two different regions of each sample.

III. RESULTS

Figure 1 shows the experimental DTA curve for SiO_2–Ga_2O_3–K_2O; two main differently structured bumps are detectable in the temperature range 600–1050 °C. The first structure, observed at about 650 °C, is attributed to the glass transition temperature (T_g) of the system; this value is consistent with the literature data for ternary galliosilicate glass.[21] The second exothermic band, which is much broader and more structured, occurs in the temperature range 700–950 °C, and peaks at about 850 °C. It could be related to a nucleation process involving gallium oxide, as we will see by analyzing the XRD data.

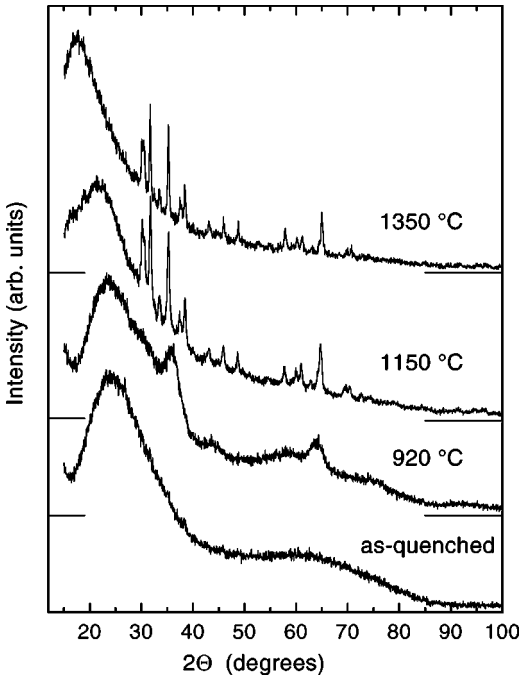

FIG. 2. Linear plot of the XRD patterns of glass samples annealed at different temperatures. The base lines of the different spectra are reported on the right-hand side.

XRD spectra of the samples annealed at different temperatures are plotted in Fig. 2. The diffraction spectrum of the as-quenched glass exhibits two very broad bands in the range 15°–100°, which are typical of glass systems. In samples annealed at 920 and 1150 °C a crystalline monoclinic β-Ga_2O_3 phase was also detected. The mean crystallite size, calculated by means of the Warren–Auerbach method, increases from ~2–3 nm at 920 °C, to ~13 nm at 1150 °C. Finally, the XRD spectrum of the sample treated in the thermobalance oven at 1350 °C, shows the presence of β-Ga_2O_3 crystallites with mean diameters of 20–25 nm. No other crystalline phase was identified in our annealed samples. Due to the small amount of material available to measurements, the diffraction spectrum of the sample treated at 1350 °C in the thermobalance oven shows a strong band peaked at 18° (2-theta) which is due to the polybutadiene-based adhesive used as sample holder.

Figure 3 is a TEM micrograph showing the microstructure of the as-quenched glass. Several particles of the as-quenched glass powder were sampled by TEM. Selected area diffractions (SAD) patterns did not reveal any crystalline reflection but the typical halo of amorphous systems. Very fine rings were detected in SAD patterns of the sample heated at 920 °C (Fig. 4). Unfortunately, the analysis of SAD patterns did not allow for an unambiguous phase identification. The micrograph in Fig. 5 shows the coherently scattering domains, which are uniformly distributed inside the amorphous matrix; this suggests that, at this annealing stage, crystalline nucleation has already occurred within the sample. The estimated crystallite size ranges from ~4 to ~10 nm. A crystal-

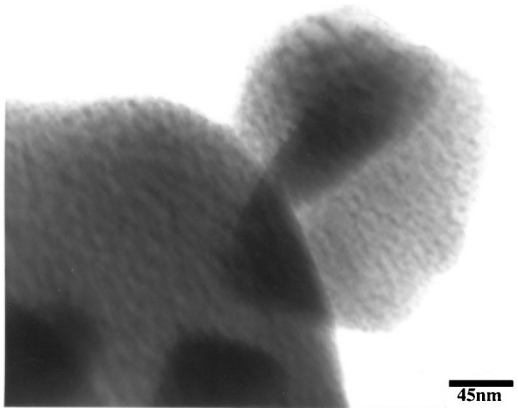

FIG. 3. TEM micrograph showing the microstructure of the as-quenched glass.

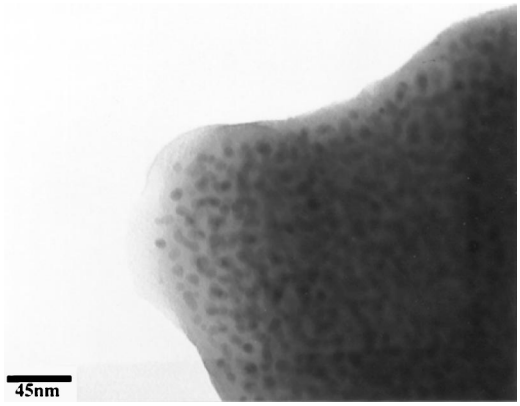

FIG. 5. TEM micrograph showing the sample microstructure after thermal treatment at 920 °C.

line phase, identified as a monoclinic β-Ga_2O_3, was detected in the glass annealed at 1150 °C. An amorphous structure is still present, as proved by the diffuse halo visible in the electron diffraction patterns. The microstructure of the sample reveals the presence of two sets of particles with different sizes within the glass matrix: a homogeneous distribution of small particles, with typical crystallite sizes of ~5 nm, coexists with larger grains, with sizes in the range 15–40 nm (Fig. 6). These TEM observations confirm the XRD results: in samples annealed at 920 °C, small-size crystals of β-Ga_2O_3 nucleate, while crystals of larger size grow in samples treated at 1150 °C.

Figure 7 shows the VV polarized Raman spectra carried out at room temperature from as-quenched glass and from some samples treated at different temperatures. The as-quenched glass shows a Raman spectrum typical of oxide glasses. The main bands are: a depolarized boson peak with maximum at about 60 cm^{-1}, a polarized broad band with maximum at about 450 cm^{-1} mainly due to O–Si–O rocking modes of SiO_4 tetrahedra, and the Si–O stretching bands in the region 800–1200 cm^{-1}.[22] There is no evidence of Raman bands due to Ga–O bonds. In fact, the bands attributed to rocking modes of GaO_4 tetrahedra and to Ga–O stretching vibration, occurring in the wave number ranges 400–550 and 500–650 cm^{-1}, respectively, in glasses containing Ga_2O_3, were previously reported as being quite weak.[23–25] The Raman spectrum of the sample annealed at 650 °C is very similar to that of the as-quenched glass. After annealing at 870 °C, in VV polarization a strong low-frequency peak appears in the spectral region of the boson band, at ~40 cm^{-1}. This peak is also present in the VV spectrum of sample annealed at 920 °C, but disappears after thermal treatments above 1000 °C. In fact, Raman spectra of these samples show many sharp peaks superimposed onto the broad bands of the glass matrix. The sample annealed at 1150 °C exhibits a strong low-frequency scattering continuum, which results into an extended tail of the elastically scattered light (Rayleigh component). Figure 8(a) compares the VV polarized spectrum of sample annealed at 920 °C with that of the as-quenched glass. The normalization factor of these two spectra was determined by superimposing their intensities in the region around 1000 cm^{-1}. Apart for the presence of an intense peak centered at ~37 cm^{-1}, the two Raman spectra are

FIG. 4. Selected area diffraction pattern of the sample annealed at 920 °C: thin diffraction rings are visible.

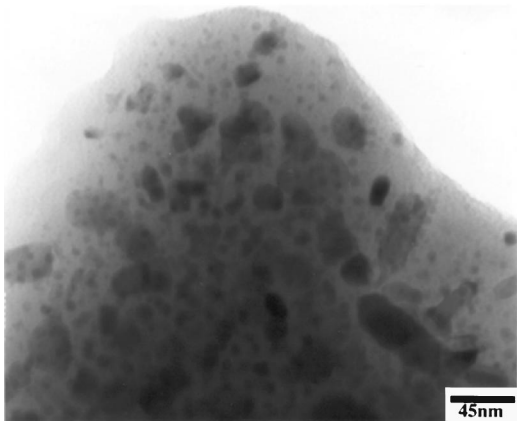

FIG. 6. TEM micrograph of the sample annealed at 1150 °C: two sets of particles are clearly observable.

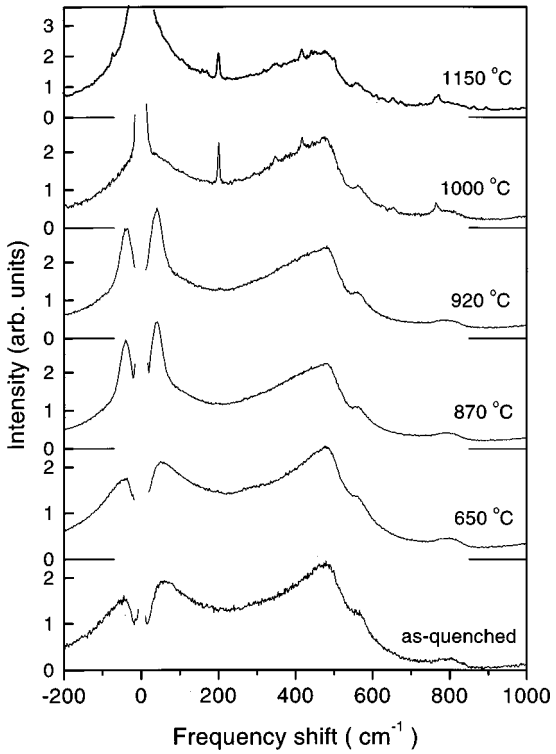

FIG. 7. VV polarized Raman spectra of as-quenched glass and samples treated at different temperatures.

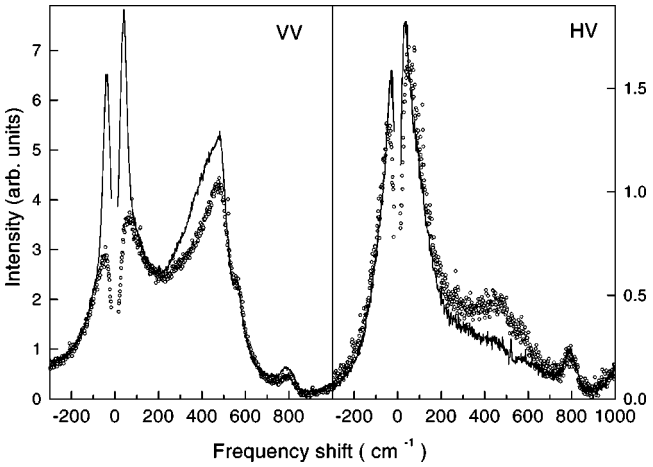

FIG. 8. (a) VV and (b) HV polarized Raman spectra of the as-quenched glass (open circles) and of the glass annealed at 920 °C (solid lines).

quite similar. The comparison of the spectra recorded from the same samples in HV polarization [Fig. 8(b)] shows the presence of a weak peak at ~25 cm^{-1} in the sample annealed at 920 °C. The noticeable difference between the two HV polarized Raman spectra in the region 300–600 cm^{-1} [see Fig. 8(b)] is probably due to a spurious effect; in fact, the exciting beam is partially depolarized inside these samples due to their poor optical quality. This causes a spillover effect. i.e., the HV (or VV) spectrum contains some VV (or HV) scattering contribution. Since the optical quality of sample annealed at 920 °C is better than that of as-quenched glass, there is a weaker spillover effect in the thermally treated sample.

IV. DISCUSSION

DTA measurements on SiO_2–Ga_2O_3–K_2O glass show an exothermic reaction in the region 800–900 °C. XRD and TEM data from the sample annealed at 920 °C evidence the nucleation of β-Ga_2O_3 nanocrystals within the glass matrix, with a mean diameter of less than 5 nm. Sample annealing at higher temperatures produces a growth of the nucleated particles. In particular, after thermal treatment at 1150 °C, β-Ga_2O_3 crystals with dimensions ranging between 15 and 40 nm are observed. They coexist, however, with nanocrystals of smaller dimensions.

Raman spectra from samples annealed at temperatures higher than 800 °C reveal the presence of nanocrystals embedded in a glass matrix, and provide precise information on their size. In fact, we attribute the low frequency scattering peaks observed in the sample annealed at 920 °C, to the acoustic vibrations of Ga_2O_3 nanoparticles dispersed in the glass matrix. Similar low-frequency structures were observed in several composite systems where dielectric,[8], semiconductor,[13,26] or metallic[27] particles are embedded into transparent vitreous matrices.[28]

Within a simplified model that considers the vibrations of a free sphere made of a continuum isotropic elastic medium, two kinds of acoustic modes are expected to be Raman active: the $l=0$ and $l=2$ spheroidal vibrations, respectively.[28,29] The $l=0$ surface vibration symmetric modes are active only in VV polarization[29] and have frequencies given by

$$\omega_0 = A_0 v_l / 2rc, \tag{1}$$

where v_l is the longitudinal sound velocity, A_0 is a constant which depends on the ratio between the transverse and longitudinal sound velocities, c is the velocity of light in vacuum, and $2r$ is the diameter of the sphere. To apply this model to a nanocrystalline cluster, a value of v_l averaged over the different crystalline directions should be considered.

The $l=2$ surface quadrupolar vibrations are active both in VV and HV polarizations,[29] with frequencies

$$\omega_2 = A_2 v_t / 2rc, \tag{2}$$

where v_t is the transverse sound velocity. Therefore, on the basis of the ratio of the Raman peak intensities in HV and VV polarizations (or the depolarization ratio), we are able to assign the Raman spectra to symmetrical ($l=0$) or quadrupolar ($l=2$) vibrations. Moreover, from the frequency position of the maximum and from the line shape of the Raman peak, it is possible to derive the mean size and the size distribution of the vibrating spherical clusters, by using Eq. (1) or (2) and by taking into account the particle-size dependence of the Raman scattering cross section.[28,30]

In order to isolate the contribution of the nanoclusters acoustic vibrations, it is necessary to subtract the Raman scattering contribution of the glass matrix, since it also presents a peak (the boson peak) in the wave number range of interest. This operation cannot be performed in a simple way because the Raman spectra of the annealed and of the as-quenched glasses are not the same. In particular the normalized spectral intensity of the VV polarized broadband cen-

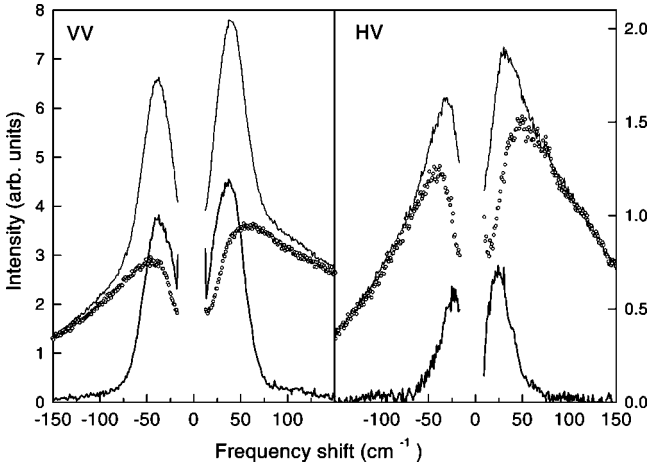

FIG. 9. (a) VV and (b) HV polarized Raman spectra of the glass annealed at 920 °C (upper solid lines) and of the as-quenched glass after correction for spillover effects between the two polarizations (open circles). The lower solid lines are the related difference spectra.

tered at about 500 cm^{-1}, assigned to the rocking modes of the silica backbone, is stronger in the annealed glass than in the as-quenched one. The two glasses have different structures since the crystalline nucleation reduces the Ga_2O_3 content in the glass matrix. Another difficulty arises from the fact that the optical quality in the untreated sample is rather poor and, as discussed above, an important spillover is observed especially in the depolarized spectra, as seen in the HV spectrum of Fig. 8 in the region around 500 cm^{-1}. The HV (VV) spectrum was corrected by subtracting a proper fraction of the VV (HV) spectrum, obtained from the same sample. After this procedure, the HV spectrum of the as-quenched glass and of the annealed samples could be reasonably superimposed in the spectral region 300–1000 cm^{-1}. Finally, the spectra of the as-quenched sample were subtracted from those of the annealed one, thus obtaining the contribution originating from the nanocluster vibrations. Figure 9 shows the results of this procedure on the spectra taken with higher resolution in a smaller wave number range, from -150 cm^{-1} (anti-Stokes side) to $+150$ cm^{-1} (Stokes side). It should be noted that the procedure assumes that the Raman spectra of the two glasses have the same shape and intensity in the boson peak spectral region. This is most probably not true. However, systematic errors could appreciably affect the result in the case of the HV spectrum, but not in the case of the VV, where the particle peak has a much stronger intensity than the boson peak.

As presented in Fig. 9, in HV polarization (a) a peak centered at 25 cm^{-1} is observed with a full width half maximum (FWHM) of $\sim$23 cm^{-1}, while in VV polarization (b) a peak centered at 37 cm^{-1} with a FWHM of $\sim$36 cm^{-1} is observed. For graphical reasons the intensity scales in Figs. 9(a) and 9(b) are not the same: actually, the VV peak is about 6 times more intense than the HV. On the basis of the results presented here we suggest that both symmetric and quadrupolar vibrations of β-Ga_2O_3 nanocrystals are observed. Symmetric vibrations are Raman active only in VV polarization and produce the intense VV peak [Fig. 9(a)]. Quadrupolar vibrations, observed in the HV spectrum [Fig. 9(b)], should appear in both spectra, but their VV contribution is probably hidden by the low frequency tail of the far more intense peak due to the symmetric vibrations [Fig. 9(a)]. If these assumptions are correct, from Eqs. (1) and (2) it can be found that the frequency ratio of the peaks in VV and HV spectra should be $\omega_{VV}/\omega_{HV}=\omega_0/\omega_2=(A_0/A_2)(v_l/v_t)$. To our knowledge the sound velocities of β-Ga_2O_3 have not been measured. They can be roughly estimated by comparison with similar oxide compounds, to be $v_l \sim 9\times10^3$ and $v_t \sim 6\times10^3$ m/s. Using these values we find: $A_0=0.72$, $A_2=0.84$, $\omega_{VV}/\omega_{HV}=1.3$, which is a value not very far from the measured frequency ratio of the two peaks, i.e., 1.5. From Eqs. (1) and (2) a nanocrystal mean size $\langle d\rangle$ (diameter of the sphere) of about 5 nm is obtained.

A more exhaustive analysis of the above results should consider the homogeneous broadening and the shift of the Raman peaks due to the interaction of the particles with the glass matrix and the size distribution of the particles, as suggested in Ref. 28. Both a Gaussian and a log-normal distribution were used to fit the line shape of the Raman peaks. The two distribution gave similar results: $\langle d\rangle=3.8$ nm and $\sigma_d=0.8$ nm, where σ_d is the standard deviation of a Gaussian distribution of particle size around the mean diameter $\langle d\rangle$. The model provides a smaller mean size ($\langle d\rangle=3.8$ nm) than that ($\langle d\rangle=5$ nm) directly obtained from Eqs. (1) and (2) by using the peak positions $\omega_0=37$ or $\omega_2=25$ cm^{-1}. This is due to the fact that the Raman intensities of the particle modes are proportional to volume of the particles themselves: different Raman weights produce an inhomogeneous Raman line shape with a maximum of the amplitude which does not correspond to the maximum of the size distribution. Unfortunately, the lack of knowledge of the elastic parameters of Ga_2O_3 does not allow to obtain precise evaluations of the mean size and size distribution of the nanoparticles, whose values scale proportionally to the inverse of sound velocity.

We did not observe the low frequency Raman peaks in the glass annealed at 1150 °C. However, we believe that in this sample a strong Raman scattering is present at very low wave numbers ($\omega<5$ cm^{-1}), which is not resolved from the elastic scattering. The reason could be the high frequency tail of a peak due to vibrations of large particles. Particles with a diameter of 15 nm (or 40 nm), as revealed by TEM and XRD analyses, should present surface modes at the wave numbers $\omega_0 \sim 12$ (or 4.5 cm^{-1}) and $\omega_2 \sim 8$ cm^{-1} (or 3 cm^{-1}), respectively. In this wave number range our experimental apparatus should be able to resolve a peak from the elastic line. However, in the presence of a large distribution of particle sizes, an important broadening and shift of the peak towards low frequency is expected. This could explain the observation of a strong increase of the Raman intensity towards the elastic line, without the presence of any observable peak.

V. CONCLUSIONS

We have investigated the nucleation and crystallization processes in the glass matrix using different experimental techniques. Nucleation of β-Ga_2O_3 nanocrystals, with sizes smaller than 5 nm occurs at temperatures close to 900 °C.

Annealing at higher temperatures induces the growth of β-Ga_2O_3 crystals of gradually increasing sizes. The surface acoustic vibrations of the nanoclusters are observed by Raman spectroscopy. From the shape of the Raman peaks we can deduce the mean size and the width of the nanoclusters size distribution; the calculated values are in agreement with those obtained by direct TEM observations and by XRD measurements, using the Warren–Auerbach method.

[1] F. Auzel, K. E. Lipinska-Kalita, and P. Santa-Cruz, Opt. Mater. **5**, 75 (1996).
[2] K. E. Lipinska-Kalita, F. Auzel, and P. Santa-Cruz, J. Non-Cryst. Solids **204**, 188 (1996).
[3] S. J. L. Ribeiro, P. Dugat, D. Avignant, and J. Dexpert-Ghys, J. Non-Cryst. Solids **197**, 8 (1996).
[4] C. Srohhöfer, J. Fick, H. C. Vasconcelos, and R. M. Almeida, J. Non-Cryst. Solids **226**, 182 (1998).
[5] M. Mortier and F. Auzel, J. Non-Cryst. Solids **256&257**, 361 (1999).
[6] G. C. Righini, M. Bettinelli, M. Brenci, C. Duverger, M. Ferrari, M. Fossi, M. Montagna, S. Pelli, and A. Speghini, Proc. SPIE **49**, 755 (1999).
[7] C. Tosello, S. Ronchin, E. Moser, M. Montagna, P. Mazzoldi, F. Gonella, M. Ferrari, C. Duverger, R. Belli, and G. Battaglin, Philos. Mag. B **79**, 2103 (1999).
[8] E. Duval, A. Boukenter, and B. Champagnon, Phys. Rev. Lett. **56**, 2052 (1986).
[9] K. E. Lipinska-Kalita and G. Mariotto, J. Non-Cryst. Solids **128**, 285 (1991); J. Mol. Struct. **267**, 241 (1992).
[10] H. B. Lal and N. Dar, Phys. Chem. Solids **38**, 161 (1977).
[11] F. Rossi, G. Pucker, M. Montagna, M. Ferrari, and A. Boukenter, Opt. Mater. **13**, 373 (2000).
[12] K. E. Lipinska-Kalita, G. Mariotto, and A. Fontana, J. Phys. IV C4-469 (1994).
[13] K. E. Lipinska-Kalita, G. Mariotto, and E. Zanghellini, Philos. Mag. B **71**, 547 (1995).
[14] J. L. Piguet and J. L. Shelby, J. Am. Ceram. Soc. **68**, C232 (1985).
[15] J. C. Lapp and J. E. Shelby, J. Am. Ceram. Soc. **69**, 126 (1986).
[16] J. C. Lapp and J. E. Shelby, Adv. Ceram. Mater. **1**, 174 (1986).
[17] P. L. Highby, J. E. Shelby, J. C. Phillips, and A. D. Legrand, J. Non-Cryst. Solids **105**, 139 (1988).
[18] J. L. Piguet and J. L. Shelby, Adv. Ceram. Mater. **1**, 192 (1986).
[19] K. E. Lipinska-Kalita and E. Gorlich, Jr., J. Non-Cryst. Solids **107**, 73 (1988).
[20] K. E. Lipinska-Kalita and D. J. Mowbray, J. Non-Cryst. Solids **122**, 1 (1990).
[21] A. Buri, D. Caferra, F. Branda, and A. Marotta, Phys. Chem. Glasses **23**, 37 (1982).
[22] F. L. Galeener, Phys. Rev. B **19**, 4292 (1979).
[23] F. Miyaji and S. Sakka, J. Non-Cryst. Solids **134**, 77 (1991).
[24] D. A. McKeown and C. I. Merzbacher, J. Non-Cryst. Solids **183**, 61 (1995).
[25] A. Mogus-Milankovic, K. Furic, C. S. Ray, W. Huang, and D. E. Day, Phys. Chem. Glasses **38**, 148 (1997).
[26] B. Champagnon, B. Andrianasolo, and E. Duval, J. Chem. Phys. **94**, 5237 (1991).
[27] M. Ferrari, L. M. Gratton, A. Maddalena, M. Montagna, and C. Tosello, J. Non-Cryst. Solids **191**, 101 (1995).
[28] M. Montagna and R. Dusi, Phys. Rev. B **52**, 10080 (1995).
[29] E. Duval, Phys. Rev. B **46**, 5795 (1992).
[30] M. Ferrari, F. Gonella, M. Montagna, and C. Tosello, J. Appl. Phys. **79**, 2055 (1996).